Communications in
Analysis and Geometry
Volume 31, Number 3, 563–593, 2023

Embedded totally geodesic surfaces in fully augmented links

Sierra Knavel and Rolland Trapp

This paper studies embedded totally geodesic surfaces in fully augmented link complements. Not surprisingly, there are no closed embedded totally geodesic surfaces. Non-compact surfaces disjoint from crossing disks are seen to be punctured spheres orthogonal to the standard cell decomposition, while those that intersect crossing disks do so in very restricted ways. Finally we show there is an augmentation of any checkerboard surface in which that surface becomes totally geodesic.

1. Introduction

The process of augmenting a link, introduced in [2], consists of placing a trivial component around two twisted strands in the link. Fully augmenting a link starts with a twist-reduced diagram, augments every twist region and removes all full twists. The complement of a fully augmented link (FAL) admits a standard cell decomposition that allows it to be realized as two right-angled, ideal polyhedra (see Section 2). The relatively straightforward

geometry of FALs, then, makes them an appealing class of links to study. Additionally, general hyperbolic links can be retrieved from FALs through Dehn filling the added trivial components. As a consequence, the relatively transparent geometry of fully augmented links can be used to study that of hyperbolic links in general (see [19]).

Normal surface theory has been successfully applied to FAL complements, obtaining results on hyperbolic links. Blair, Futer and Tomova use normal surface theory to bound the genera of certain surfaces in highly twisted link complements (see [7]). Futer and Purcell, in [11], apply normal surface theory and combinatorial arguments to show highly twisted links admit no exceptional surgeries, while Kalfagianni and Lee use normal surfaces to bound crosscap numbers of alternating links (see [13]). In each of these contexts the authors topologically "straighten" surfaces relative to a polyhedral decomposition of the link complement. The polyhedra then decompose the surface into a collection of normal disks that glue together to form the original surface.

In addition to topological considerations, it is natural to study surface geometry in the context of hyperbolic three manifolds. The purpose of this paper is to study embedded totally geodesic surfaces in FAL complements. A geometric version of normal surface theory is used, the main tool being *geodesic disks* which are geometric analogues of the normal disks of [7], [11], and [13]. These are defined in Section 4, where properties are also developed which greatly restrict how such surfaces can intersect crossing disks (see Proposition 4.3).

Much work has been done on the (non-)existence of totally geodesic surfaces in hyperbolic three-manifolds. Moreover, various properties of geodesic surfaces are frequently compared: immersed vs. embedded, closed vs. non-compact, orientable vs. non-orientable, etc.

One need look no farther than the figure-eight knot to see that the distinction between immersed and embedded is significant. The figure-eight knot complement is an arithmetic manifold containing infinitely many *immersed* closed totally geodesic surfaces (see [21]). At the other end of the spectrum, Menasco and Reid, in [17], proved there are no *embedded* closed geodesic surfaces in the complement of hyperbolic alternating links in S^3. Therefore, none of those infinitely many surfaces are embedded!

It seems that closed embedded totally geodesic surfaces are rare. In fact, Menasco and Reid conjectured that knots in S^3 never contain such a surface. This conjecture has been proven for a range of knot families, including closed four braids ([16]), 3-bridge and double-torus knots ([12]), and almost-alternating links ([4]). In contrast to knots, Menasco and Reid

provide an example of a link complement containing a genus two closed embedded totally geodesic surface (see [17, Section 2.3]). Our first result shows that while some links do contain surfaces that are closed, embedded and geodesic, FAL complements do not. More formally, we prove

Theorem 3.1. *There are no closed, embedded, totally geodesic surfaces in an FAL complement.*

The proof relies on the standard decomposition of FAL complements into two right-angled, ideal polyhedra (described in Section 2), together with how embedded, totally geodesic surfaces can intersect thrice-punctured spheres.

Although FAL complements contain no closed embedded totally geodesic surfaces, they do contain non-compact ones. Both the reflection surface and crossing disks of the standard cell decomposition provide examples of embedded totally geodesic surfaces (see [19] and [14]). These will be referred to as *standard* geodesic surfaces. In general, FAL complements contain *non-standard* embedded totally geodesic surfaces as well. Non-standard surfaces are characterized by their intersections with the standard ones. Such an analysis on surfaces disjoint from crossing disks proves

Theorem 3.3. *Let S be a non-standard surface in an FAL complement that is connected and disjoint from the crossing disks. Then S is an n-punctured sphere orthogonal to the reflection surface.*

Technical results regarding geodesic disks are developed in Section 4, and used to characterize embedded, totally geodesic surfaces that intersect crossing disks:

Theorem 5.1. *Let S be a connected, non-standard surface in an FAL complement that intersects at least one crossing disk. Then either*

i. S meets crossing disks only in separating geodesics and is orthogonal to the standard cell decomposition, or

ii. S meets crossing disks only in non-separating geodesics and is nowhere orthogonal to $\mathcal{C}$.

Several examples are given as applications of these results. In particular, Example 5.2 classifies embedded, totally geodesic surfaces in flat FALs that come from augmenting two-bridge links. Given a two-bridge link with n twist regions, its corresponding flat FAL contains $3n+2$ or $3n+3$ embedded, totally geodesic surfaces if n is even or odd, respectively. These FALs are octahedral, and so arithmetic by [9, Proposition 6.3]. Thus these are also

examples of manifolds containing infinitely many closed, but only finitely many embedded, totally geodesic surfaces.

All examples of orientable, embedded, totally geodesic surfaces we have constructed that are orthogonal to the standard cell decomposition have been punctured spheres. Thus we conjecture

Conjecture 1.1. Any orientable, embedded, totally geodesic surface in an FAL complement that is orthogonal to the standard cell decomposition has genus zero.

After analyzing non-standard surfaces, we turn our attention to standard ones. In particular, we are interested in the types of surfaces that can be reflection surfaces in an FAL complement. Surfaces such as Seifert surfaces, checkerboard surfaces, and state surfaces, arise naturally when considering links in S^3, and several authors have studied the geometry of such surfaces. Adams and Schoenfeld, in [5], constructed the first examples of totally geodesic Seifert surfaces, as well as proving that hyperbolic two-bridge knot complements contain no orientable totally geodesic surfaces. More totally geodesic Seifert surfaces were found in [3], where the authors also show that if both checkerboard surfaces of an alternating link diagram contain bigons, then neither are totally geodesic. Futer, Kalfagianni and Purcell, in [10], showed that state surfaces, and in particular checkerboard surfaces, of alternating diagrams are always quasi-Fuchsian. A quasi-Fuchsian surface is one covered by a topological plane with limit set a topological circle that bounds two disks. A totally geodesic (or Fuchsian) surface satisfies this definition, since the limit set of a hyperbolic plane is a geometric circle, which is certainly a topological circle.

While not all checkerboard surfaces are totally geodesic, we define an augmentation $\mathcal{A}_R$ of a checkerboard surface R in which it becomes totally geodesic. The following theorem is proven using Purcell's classification of hyperbolic FALs (restated as Theorem 2.1 in this paper for convenience), together with a diagrammatic analysis of related links:

Theorem 6.2. *Let R be a checkerboard surface for a nonsplittable, prime, twist-reduced diagram D with at least two twist regions. Then R is an embedded totally geodesic surface in the complement of the hyperbolic link $\mathcal{A}_R$.*

The present work restricts its attention to the study of embedded totally geodesic surfaces. Fully augmented links are reviewed in Section 2. Section 3

contains Theorems 3.1 and 3.3, while Section 4 develops the necessary structure of geodesic disks. Section 5 characterizes non-standard surfaces that intersect crossing disks, and classifies embedded, totally geodesic surfaces for an infinite family of links. The paper concludes in Section 6 by showing that the correct augmentation of a checkerboard surface results in it becoming totally geodesic.

We remark that these results have been used in [18] to classify thrice-punctured spheres in FAL complements and analyze their belted-sum decompositions. Further, there are potential applications to arithmetic invariants, which are well-behaved under such cut-and-paste operations (see [15]).

Acknowledgements. We are very grateful to the anonymous referees for their careful reading and valuable suggestions that resulted in a significantly improved version of this paper. This research was supported in part by NSF-REU Grant DMS-1461286, as well as California State University, San Bernardino.

2. Fully augmented links

This section introduces fully augmented links, their standard cell decomposition and associated ideal polyhedra. These tools form the foundation for our analysis of embedded totally geodesic surfaces in FAL complements. The reader is referred to Purcell's paper [19] for a thorough discussion of these ideas.

Fully augmented links are obtained from alternating diagrams of links in the three-sphere, so before continuing we briefly recall the definitions of some diagrammatic properties.

A diagram is *nonsplittable* if every disk whose boundary is disjoint from the diagram contains either all or none of the diagram. To define prime, recall that an m-tangle in a diagram is a disk whose boundary intersects the diagram in exactly m points, none of which are crossings (see [8]). A trivial 2-tangle is one that contains either all or none of the crossings in the diagram (see Figure 1(a)). A diagram is *prime* if every 2-tangle is trivial. Finally, a prime diagram is *twist-reduced* if for each pair S and T of 4-tangles whose complement contains two crossings as in Figure 1(b), either S or T contains a (possibly empty) twist.

We now describe how to construct an FAL. Given a twist-reduced alternating link diagram L in S^3 one forms its associated fully augmented link $\mathcal{A}_L$ by inserting a trivial component, called a *crossing circle*, around each

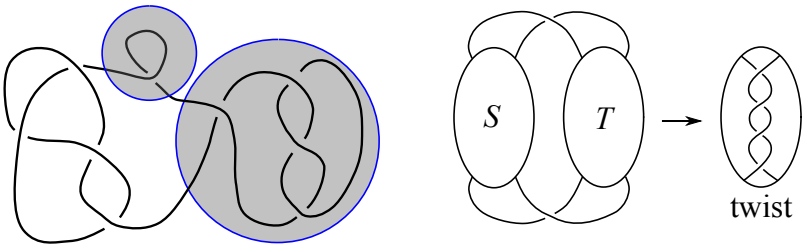

(a) Non-trivial 2-tangles (b) Twist-reduced implies either S or T is a twist

Figure 1: Diagrammatic properties.

twist region and removing all full twists (see Figure 2). The components remaining from the original link are called *knot circles*.

Two remarks are in order. First, note that if a twist region contains a single crossing there are two choices for crossing circles, as is the case for the central crossing of Figure 2(a). A multiple-crossing twist region, however, determines a unique crossing circle. Second, observe that each crossing circle bounds a *crossing disk* that is punctured twice by knot circles, so that each crossing disk is a thrice-punctured sphere. A crossing circle is *flat* if the knot circles through it do not cross, and it is called *twisted* if they do. The left two crossing circles of Figure 2(b) are twisted while the right two are flat.

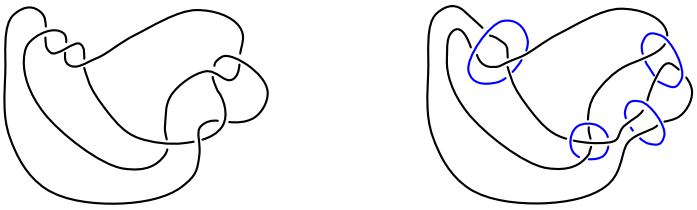

(a) Alternating link (b) Fully augmented

Figure 2: Fully augmenting a link.

Purcell gives a diagrammatic interpretation of when the associated FAL complement admits a hyperbolic structure. This theorem is included here for reference.

Theorem 2.1 ([19, Theorem 2.5]). *A fully augmented link is hyperbolic if and only if the associated knot or link diagram is nonsplittable, prime, twist-reduced, with at least two twist regions.*

Each hyperbolic fully augmented link, or FAL, admits a *standard cell-decomposition* first introduced in the appendix of [14], which allows one to realize the complement $M = S^3 \setminus \mathcal{A}_L$ as two right-angled ideal polyhedra (see [19]). We let $\mathcal{C}$ denote the standard cell decomposition, and describe it now.

The standard cell decomposition is most easily seen when all crossing circles are flat, so we begin with this case. There are two kinds of 2-cells in $\mathcal{C}$: the regions of the projection plane (e.g. U and V in Figure 3(a)) and the crossing disks. We refer to the projection plane 2-cells as *reflection 2-cells* since reflection across the plane of projection is a symmetry of the link $\mathcal{A}_L$. Note that the crossing disks are preserved under this reflective symmetry. The 2-cells from crossing disks are *crossing 2-cells*. The projection plane cuts through the middle of each crossing disk, and the curves of intersection are the 1-cells of the standard cell decomposition (see the line segments of Figure 3(a)). Crossing disks are cut into two triangles by the 1-cells, one above and one below the plane of projection (e.g. A, A' in Figure 3(a)) .

There are no 0-cells in the standard cell decomposition as all 1-cells have "endpoints" on the link $\mathcal{A}_L$, which is absent from M. The two 3-cells $B^3_\pm$ correspond to the regions of M above and below the projection plane.

To realize the hyperbolic structure on M, first slice along the reflection 2-cells in $\mathcal{C}$. This separates M into the two 3-cells with boundary, which are reflections of each other. Cutting along the projection plane slices each crossing disk in half, so each crossing disk contributes one triangle in each 3-cell. Since the 3-cells are reflections of each other, we focus on the portion above the reflection plane in Figure 3(a).

Now slice along the half-crossing disks, and flatten the result. This yields a three ball B^3_+, whose boundary sphere (viewed from "inside" B^3_+) is pictured in Figure 3(b).

Arcs from the original link remain in ∂B^3_+, which are those arcs of Figure 3(b) that do not come from edges in the standard cell decomposition. Since these arcs correspond to part of the link they are not part of M and can be shrunk to points. The result is a cell decomposition on the boundary of B^3_+. This cell decomposition can be checkerboard colored so that the unshaded faces correspond to reflection 2-cells, while shaded faces are all triangular and copies of crossing 2-cells.

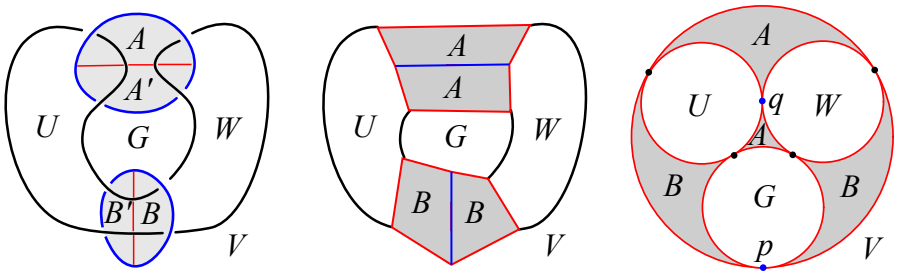

(*a*) Cell decomposition (*b*) After slicing 2-cells (*c*) Circle packing

Figure 3: The standard cell decomposition $\mathcal{C}$ and circle packing.

A consequence of Andreev's Theorem [6] is that the unshaded faces can be isotoped to form a circle packing. Two circles are tangent in the circle packing if the corresponding regions in the plane share a knot circle or are both punctured by the same crossing circle. Thus the circles corresponding to regions U and W are tangent at the vertex q corresponding to the crossing circle bounding A (see Figure 3(c)).

Moreover, the ideal polyhedron is right-angled. This follows from the fact that reflection across the plane of projection is an involution that preserves crossing disks. The involution is isotopic to an isometry fixing the plane of projection pointwise, and one consequence of Mostow-Prasad rigidity is that such a fixed point set is totally geodesic. Since the crossing disks are preserved under reflection, reflection 2-cells must meet crossing 2-cells at right angles.

By reflective symmetry, the analogous operations on the region below the plane yields an ideal right-angled polyhedron P_- which is the reflection of P_+. To find a fundamental domain for M, let P_- be the reflection of P_+ across an unshaded face G. Then $\mathcal{F} = P_+ \cup P_-$ is a fundamental domain for M, which we call a *standard domain* since is comes from the standard cell decomposition. Figure 4(a) illustrates a standard domain $\mathcal{F}$ for the Borromean rings of Figure 3(a). This is obtained by reflecting P_+ across the face labeled G in Figure 3(c) and applying a Móbius transformation that maps the vertex labeled p to infinity. Note that standard domains are not unique because of the choice of unshaded face used to create P_-, as well as choosing which vertex of $\mathcal{F}$ to map to a convenient position.

The gluing maps on the faces of $\mathcal{F}$ are quite explicit. To describe the gluings between unshaded faces we refer to faces, edges and vertices of $\mathcal{F}$

that are reflections of each other as *corresponding* faces, edges or vertices, respectively. If F and F' are corresponding unshaded faces, then they are glued by identifying corresponding edges and vertices. This is realized by the isometry $r_G \circ r_F : F \to F'$, where r_F and r_G represent reflections across the respective faces (recall that G is the shared face of $P_\pm$). Indeed, reflection in F fixes F point-wise while reflection in G identifies corresponding components of F and F'.

For a flat FAL, each shaded triangle on P_+ will be glued to an adjacent shaded triangle by the parabolic isometry that fixes their shared point (for example, the point q between the triangles labeled A in Figure 3). Shaded triangles on P_- are identified in similar fashion.

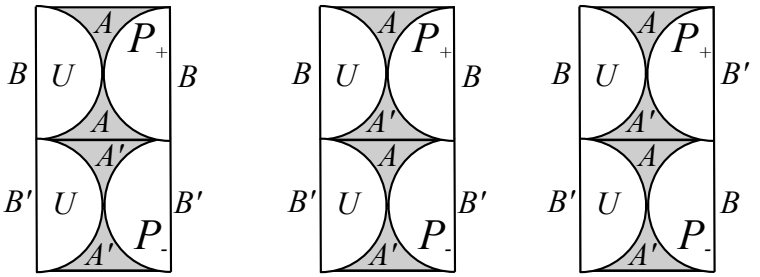

(*a*) Borromean Rings (*b*) Twisted A (*c*) Both twisted

Figure 4: Comparing flat and twisted gluing patterns.

To see how twisted crossing circles change the above description, note that a twisted crossing circle can be obtained from a flat one by slicing along the crossing disk and regluing with a half-twist. This glues the top and bottom of one copy of the crossing disk to the bottom and top of the other. Carrying the projection plane along in the process yields the reflection 2-cells which form a reflection surface for the twisted disk. The reflection is the homeomorphism defined by reflecting in the plane of projection followed by full twists inside each twisted crossing circle.

Note that the polyhedra $P_\pm$ are the same for the half-twist, but shaded triangles in opposite polyhedra are identified. For example, the gluing pattern on the standard domain of Figure 4(*b*) results from twisting crossing disk A. Shaded triangles corresponding to crossing disk A are identified across $P_\pm$ while those corresponding to disk B are glued within each polyhedron. Figure 4(*c*) is a standard domain for the Borromean rings with both crossing disks twisted.

As mentioned above (or see [19, Lemma 2.1]) the 2-cells of $\mathcal{C}$ are pieces of embedded totally geodesic surfaces in the FAL complement. For this reason we call the crossing disks and reflection surfaces *standard* geodesic surfaces in M.

3. Embedded geodesic surfaces

This section begins our study of embedded totally geodesic surfaces in FAL complements. The standard cell decomposition $\mathcal{C}$ of Section 2 is used to prove that FAL complements contain no closed, embedded, totally geodesic surfaces in Theorem 3.1. Embedded, totally geodesic surfaces that are disjoint from crossing disks are then considered. Analyzing intersections in a standard domain proves that such surfaces are always punctured spheres orthogonal to $\mathcal{C}$ (see Theorem 3.3).

A surface S in a hyperbolic FAL complement M is *totally geodesic* if its preimage $\widetilde{S}$ in the universal cover $\widetilde{M} = \mathbb{H}^3$ is a union of hyperbolic planes. If in addition S is embedded, then the planes of $\widetilde{S}$ are pairwise disjoint. Observe that the intersection of two distinct, embedded, totally geodesic surfaces is a union of pairwise disjoint, simple geodesics which can be either closed or non-compact. To see this merely note that the intersection of two such surfaces is transverse, so the local picture near any point of intersection is two planes intersecting along a line. This observation will be particularly useful when analyzing the intersection of embedded, totally geodesic surfaces with crossing disks.

Since crossing disks in FAL complements are embedded thrice punctured spheres, we review these now. Adams proved, in [1], that all embedded thrice-punctured spheres in orientable hyperbolic 3-manifolds are isotopic to totally geodesic ones. For this reason we always assume our thrice-punctured spheres are totally geodesic. Furthermore, thrice-punctured spheres contain exactly six simple geodesics (see Figure 5(a)). The geodesics labeled a, b, c will be called *non-separating* geodesics since the thrice-punctured sphere is still connected after slicing along one, and those labeled x, y, z are *separating* geodesics (these are also commonly known as *seams* and *waves*, respectively).

In particular, note that closed geodesics on a thrice-punctured sphere are not simple. Thus if an embedded, totally geodesic surface intersects an embedded thrice-punctured sphere non-trivially, it is not closed. This helps in proving the following theorem.

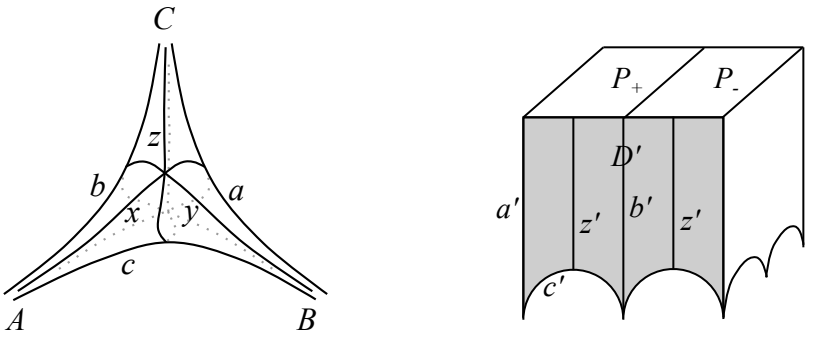

(*a*) Geodesics on D (*b*) A standard domain $\mathcal{F}$

Figure 5: Thrice-punctured spheres and standard domains.

Theorem 3.1. *There are no closed, embedded, totally geodesic surfaces in an FAL complement.*

Proof. Let S be an embedded totally geodesic surface in an FAL complement. We use its intersection with the standard cell decomposition $\mathcal{C}$ to show that it is not closed.

If S intersects a crossing disk, it does so in complete simple geodesics which are not closed, so S is non-compact.

Before continuing with the proof we make some observations about the intersection $S \cap \mathcal{C}$. An embedded totally geodesic surface must intersect $\mathcal{C}$, otherwise it is contained in a three-ball and is inessential. Moreover, since S is essential and the 2-cells of $\mathcal{C}$ are topological disks, S cannot intersect a 2-cell in a closed geodesic. Finally, each edge of $\mathcal{C}$ is contained in a crossing disk, so if S intersects (or contains) an edge, then it intersects a crossing disk.

Now suppose S is disjoint from crossing disks. Then it must intersect only reflection 2-cells in non-closed geodesics that are disjoint from the edges of $\mathcal{C}$. Thus the intersection $S \cap \mathcal{C}$ consists of open geodesics in reflection 2-cells, and S is non-compact. □

Given the result of Theorem 3.1, we turn our attention to non-compact, embedded, totally geodesic surfaces in FAL complements. Recall that the 2-cells of $\mathcal{C}$ glue together to form *standard* geodesic surfaces in FAL complements. We make the following definition.

Definition 3.2. A *non-standard surface* is an embedded, totally geodesic surface in an FAL complement that is not a component of $\mathcal{C}$.

We first characterize non-standard surfaces that do not intersect crossing disks.

Theorem 3.3. *Let S be a non-standard surface in an FAL complement that is connected and disjoint from the crossing disks. Then S is an n-punctured sphere orthogonal to the reflection surface.*

Proof. Let M be an FAL complement and S be a surface in M that satisfies the hypotheses of the theorem. Since S misses all crossing disks, it intersects only reflection 2-cells of $\mathcal{C}$ in open geodesics, as in the proof of Theorem 3.1,.

To see that S is orthogonal to the reflection surface we show that if S is not orthogonal to it, then S intersects a crossing disk. Let p be a cusp of M that is also a puncture of S, and choose $\mathcal{F}$ to be a standard domain of M for which infinity projects to the cusp p. Then there is a vertical geodesic γ' in an unshaded vertical face of $\mathcal{F}$ that projects to one component of S intersected with the reflection surface (see Figure 6). Let S^* be the plane containing γ' that projects to S.

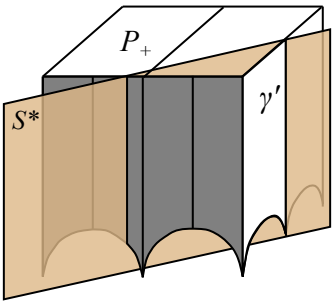

Figure 6: An elevation S^* when S is not orthogonal to the reflection surface.

Then S^* is not orthogonal to the unshaded face of $\mathcal{F}$, as S is not orthogonal to the reflection surface. This implies S^* intersects the plane containing vertical shaded faces of $\mathcal{F}$ (although the intersection is not necessarily in $\mathcal{F}$ as it is in Figure 6), and S intersects a crossing disk in M.

Thus if S is disjoint from crossing disks, it must be orthogonal to the reflection surface.

It remains to show that S is an n-punctured sphere. Now let S^* denote a vertical plane in $\mathbb{H}^3$ that covers S and intersects $\mathcal{F}$ non-trivially. Note that

$S'_+ = S^* \cap P_+$ is an ideal n-gon. Moreover, since S^* is perpendicular to the unshaded faces of P_+, it is preserved under reflection across them. Thus the intersection $S'_- = S^* \cap P_-$ is the reflection of S'_+ across the face shared by $P_\pm$.

Since unshaded faces of $\partial P_\pm$ glue to their reflections, so do the boundaries of $S'_\pm$. Thus projection of $S'_\pm$ to M is an embedded totally geodesic surface obtained by gluing the boundaries of two ideal n-gons in cyclic order, which is an n-punctured sphere. Since S is connected, it equals this surface. □

Figure 7 illustrates examples of totally geodesic punctured spheres that are disjoint from crossing disks. Applying the techniques of Section 2 to the twelve-link chain yields the circle packing of Figure 7(b), which is the footprint of P_+. The labeled curves are disjoint from shaded triangles, and represent the boundaries of hyperbolic planes S_1^*, S_2^* in the universal cover which project to embedded totally geodesic surfaces in the FAL complement.

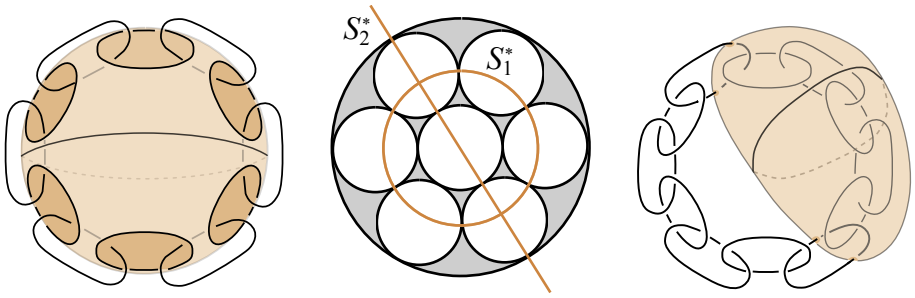

(a) All six punctures along crossing circles

(b) Planes S_1^*, S_2^*, intersecting P_+

(c) Sphere with four knot circle punctures

Figure 7: Embedded, totally geodesic surfaces that are disjoint from crossing disks.

The plane S_1^* projects to the six-punctured sphere of Figure 7(a). All six punctures are longitudes of crossing circles, so the sphere is disjoint from crossing disks. The plane S_2^* projects to the four-punctured sphere of Figure 7(c). This sphere separates three crossing disks from the other three, and is punctured four times by knot circles.

4. Geodesic disks

This section introduces geodesic disks and uses them to analyze how non-standard surfaces in FAL complements can intersect crossing disks and the reflection surface. The ways in which a non-standard surface meets crossing disks are summarized in Proposition 4.3. Further, Proposition 4.4 shows that a non-standard surface orthogonal to one 2-cell in $\mathcal{C}$ is orthogonal to every 2-cell that it meets. We begin with a definition.

Definition 4.1. Let M be an FAL complement and S an embedded totally geodesic surface in M with preimage $\widetilde{S}$ in the universal cover. A *geodesic disk* is a connected component of $\widetilde{S} \cap P_+$, or of $\widetilde{S} \cap P_-$.

Faces of the polyhedra $P_\pm$ are *standard geodesic disks* since they project to the standard cell decomposition of M.

Geodesic disks, then, are obtained by intersecting $P_\pm$ with special planes. The planes must project to embedded totally geodesic surfaces in the FAL complement. The ideal polygons $S'_\pm$ in the proof of Theorem 3.3 are examples of geodesic disks.

The following figure illustrates these concepts. The surface S of Figure 8(a) is an embedded thrice-punctured sphere, so it is an embedded geodesic surface (see [1]). Thus its preimage $\widetilde{S}$ in the universal cover is a union of disjoint planes, some of which are displayed in Figure 8(b) together with the standard domain $\mathcal{F}$. Two of the planes in $\widetilde{S}$ actually intersect $\mathcal{F}$, and the corresponding geodesic disks are depicted in Figure 8(c).

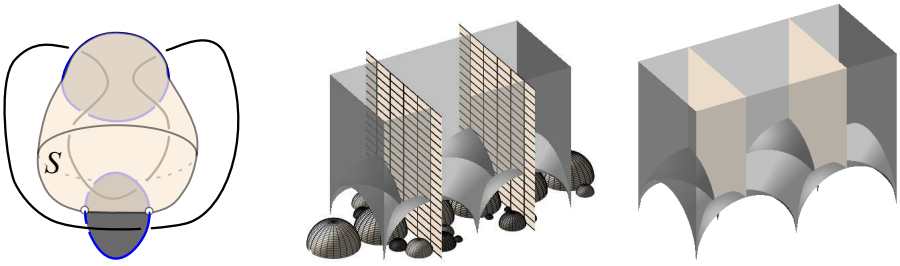

(a) 3-punctured sphere (b) $\widetilde{S}$ with $\mathcal{F}$ (c) Geodesic disks

Figure 8: A geodesic surface S, its $\widetilde{S}$, and geodesic disks.

Theorem 3.3 characterizes embedded, totally geodesic surfaces in FAL complements that are disjoint from crossing disks. We must now analyze

how these surfaces can intersect crossing disks. To do so we relate crossing disks and their simple geodesics to shaded triangular faces of a standard domain.

The preimage in a standard domain of a crossing disk D, and of its geodesics, is very specific. A longitude of the crossing circle is one puncture of D, while the other two punctures correspond to meridians of knot circles (see Figure 3(a)). The 1-cells of $\mathcal{C}$, then, connect distinct punctures and are the non-separating geodesics of the crossing disks. Thus the edges of the shaded triangles in $\partial P_{\pm}$ project to non-separating geodesics of crossing disks (e.g. the geodesics labeled a', b', c' in Figure 5(b) project to a, b, c on D).

We now describe the preimage in $\mathcal{F}$ of separating geodesics on crossing disks. Recall that an *altitude* of an ideal triangle is the result of dropping a perpendicular from one vertex to the opposite side. Since separating geodesics are perpendicular to their opposite non-separating geodesic, we see that altitudes of the shaded triangles of $\mathcal{F}$ project to separating geodesics of D. For example, the rays labeled z' in Figure 5(b) glue together and project to form z in D.

These observations reveal some of the structure of geodesic disks. In particular, if S is an embedded, totally geodesic surface in an FAL complement, then it intersects crossing disks in a union of disjoint separating and non-separating geodesics. The preimages of these geodesics in $\mathcal{F}$ are edges or altitudes of shaded triangles. Thus if a geodesic disk intersects a shaded triangle it does so along an edge or an altitude.

The next lemma describes the angles at which geodesic disks can intersect shaded triangles. Since the covering projection preserves angles, they also determine angles between embedded, totally geodesic surfaces and certain 2-cells in $\mathcal{C}$.

Lemma 4.2. *Let S be a non-standard surface in an FAL complement M, and let $\mathcal{F}$ be a standard domain for M. If S' is a non-standard geodesic disk for S that intersects a shaded triangular face T of $\mathcal{F}$, then*

i. If $S' \cap T$ is an altitude z' of T, then S' is orthogonal to both T and the unshaded face R at the base of z'.

ii. If $S' \cap T$ is an edge a' of T, then S' is not orthogonal to either face of $\mathcal{F}$ adjacent at a'.

Proof. Let S' be a geodesic disk containing the altitude z' of T, say in P_+, and assume the ideal point of z' is at infinity. Let R be the unshaded face at the finite endpoint of z' (see Figure 9).

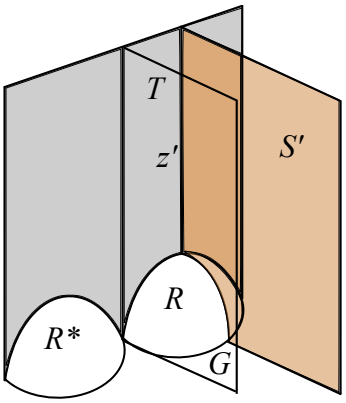

Figure 9: S' when $S \cap D$ is separating in D.

Since S' is a vertical plane containing z', it contains the center of the Euclidean hemisphere containing R. Thus S' is orthogonal to R.

We will show that if S' is not orthogonal to T, then $\widetilde{S}$ contains intersecting planes–a contradiction since S is embedded.

Let G be the face shared by $P_{\pm}$ that contains an edge of T, and let R^* be the reflection of R across G. The isometry φ gluing R to R^* is realized by first reflecting in R, then reflecting in G. Since S' is a vertical plane through the Euclidean center of the hyperbolic plane containing R, it is (set-wise) invariant under reflection in R. The image $S^* = \varphi(S')$ is therefore the reflection of S' across G.

If S' is not orthogonal to T, then it intersects G in the universal cover of M (although not necessarily in $\mathcal{F}$). The vertical line $S' \cap G$ is invariant under reflection in G, so $S' \cap \varphi(S) = S' \cap S^*$ is non-empty. This contradicts the fact that embedded totally geodesic surfaces lift to a union of disjoint planes in the universal cover. This completes the proof of the first statement.

Now suppose $S' \cap T$ is an edge a' of T, and let R be the unshaded face of P_+ sharing a' with T. Since S' is non-standard it cannot be either T or R. Since R and T are orthogonal at a', S' cannot be perpendicular to either of them. □

Lemma 4.2 can be used to describe the intersection of embedded totally geodesic surfaces with crossing disks. The following proposition summarizes this. Part (i) is a restatement of the observation that embedded, totally geodesic surfaces intersect in a union of disjoint simple geodesics. Parts (ii)

and (*iii*) follow directly from Lemma 4.2 and the fact that geodesic disks project to embedded totally geodesic surfaces.

Proposition 4.3. *Let S be a non-standard surface in an FAL complement that intersects the crossing disk D nontrivially. Then*

i. $S \cap D$ is a collection of pairwise disjoint separating and non-separating geodesics on D.

ii. S meets D orthogonally along any separating geodesic in $S \cap D$.

iii. At non-separating geodesics in $S \cap D$, S is not orthogonal to D.

The final result of this section shows that if a geodesic disk meets one face of $\partial P_{\pm}$ orthogonally, then it is orthogonal to every face it meets. To see this we first discuss the boundary of a geodesic disk. The arguments given for P_+ also apply to geodesic disks in P_-.

First recall that the midpoint of an edge in an ideal triangle is the foot of the perpendicular from the opposite vertex. Since each edge of P_+ bounds a shaded ideal triangle on one side, it has a well-defined midpoint.

Let S' be a non-standard geodesic disk, so it is a hyperbolic polygon with boundary curve γ that can have both finite and ideal vertices. The boundary curve γ intersects shaded triangles along edges or altitudes, so all finite vertices of γ are midpoints.

Proposition 4.4. *If a non-standard geodesic disk S' meets one face of ∂P_+ orthogonally, then S' is orthogonal to every face of ∂P_+ that it meets. In particular, if S' contains an altitude it is orthogonal to every face it meets.*

Proof. Let S' be a non-standard geodesic disk in P_+ and let the edges of $\gamma = \partial S'$ be labeled $\gamma_1, \ldots, \gamma_n$ in cyclic order. Let γ_i be an edge along which S' meets ∂P_+ at right angles. We wish to prove that S' is orthogonal to ∂P_+ along γ_{i+1} as well. The proof will follow by applying this argument cyclically around γ.

If γ_i and γ_{i+1} share a finite vertex, then one of the edges is an altitude and Lemma 4.2(i) proves that S' is orthogonal to ∂P_+ along both edges.

If γ_i and γ_{i+1} share an ideal vertex, map it to infinity via a Möbius transformation. Since S' is orthogonal to ∂P_+ along γ_i, and P_+ is right angled, the geodesic disk S' meets the face of P_+ opposite γ_i orthogonally as well. The face opposite γ_i contains γ_{i+1}, so S' meets ∂P_+ orthogonally along γ_{i+1}, finishing the induction. □

5. Non-standard surfaces intersecting crossing disks

Theorem 3.1 shows there are no closed, embedded, totally geodesic surfaces in FAL complements. Theorem 3.3 nicely characterizes embedded, totally geodesic surfaces in an FAL complement that are disjoint from crossing disks. This section completes the picture by considering embedded, totally geodesic surfaces that intersect crossing disks.

Recall that an embedded totally geodesic surface S intersects a crossing disk in a collection of disjoint separating and non-separating geodesics (Proposition 4.3(i)). Theorem 5.1 strengthens this to show that if S is connected, then all intersections with crossing disks are of the same type–either all are separating or all non-separating.

Theorem 5.1. *Let S be a connected, non-standard surface in an FAL complement that intersects at least one crossing disk. Then either*

i. S meets crossing disks only in separating geodesics and is orthogonal to the standard cell decomposition, or

ii. S meets crossing disks only in non-separating geodesics and is nowhere orthogonal to $\mathcal{C}$.

Proof. We begin by showing that if S meets one crossing disk in a separating geodesic then S satisfies case (i), starting with the orthogonality condition. Since S contains a separating geodesic of some crossing disk, then some geodesic disk S' for S contains an altitude. Proposition 4.4 then implies S' is orthogonal to ∂P. Now S is totally geodesic, so any geodesic disk glued to S' is also orthogonal to ∂P. Since S is connected, repeating this argument shows all geodesic disks for S meet the standard cell decomposition orthogonally. To finish the proof that S satisfies case (i), observe that Proposition 4.3(iii), combined with the fact that S is perpendicular to $\mathcal{C}$, implies it can only meet crossing disks in separating geodesics.

If S intersects a crossing disk D in a non-separating geodesic, then Proposition 4.3(iii) shows S is not orthogonal to D there. Proposition 4.4 produces a geodesic disk S' which is not perpendicular to ∂P, and a similar gluing argument to case (i) shows S is never perpendicular to $\mathcal{C}$. Of course, this implies that S cannot meet a crossing disk in a separating geodesic, and case (ii) holds. □

We remark that Figure 8 illustrates the first case of Theorem 5.1. The thrice-punctured sphere S of Figure 8(a) intersects the bottom crossing disk along a separating geodesic. Figure 8(c) illustrates that S is orthogonal

to standard geodesic surfaces in the Borromean rings. In this example the altitudes in a geodesic disk glue to each other. We now sketch an example where distinct geodesic disks glue along altitudes.

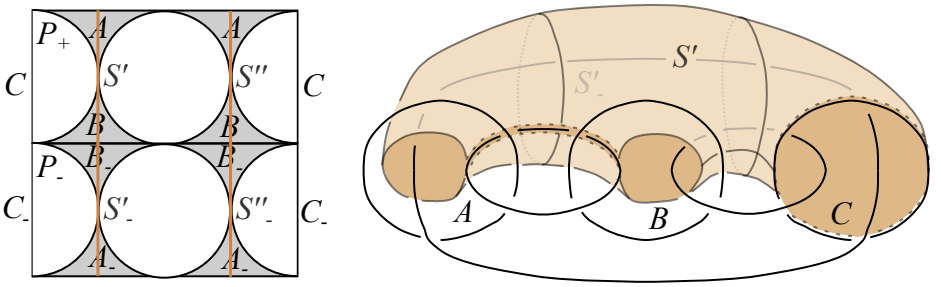

(a) Geodesic disks in $\mathcal{F}$ (b) Projection of $S' \cup S'_-$, or back half of S

Figure 10: S intersects crossing disks A, B in separating geodesics.

Figure 10(a) depicts a fundamental region for a FAL in which P_+ contains two geodesic disks S' and S''. The polyhedron P_- contains their reflections S'_-, S''_-. The prescribed gluing results in the six-component link of Figure 10(b) with crossing disks A, B, C (which are not pictured). Included in Figure 10(b) is the image of $S' \cup S'_-$, which comprises the back half of S. The front half of S is obtained by reflecting across the plane containing the crossing disks. Note that S intersects both crossing disks A and B in separating geodesics with "endpoints" on the component through A and B. The component through A and B corresponds to two punctures on S, one above and one below the projection plane. Further, the cusp corresponding to infinity in Figure 10(a) is the puncture corresponding to crossing circle C pictured in Figure 10(b).

We conclude this section with examples of embedded totally geodesic surfaces that are not orthogonal to the standard cell decomposition (the second case of Theorem 5.1). Figure 11(a) illustrates two geodesic disks in the fundamental domain for the Borromean rings. One can verify that these project to one of the checkerboard surfaces in the alternating diagram of the Borromean rings (the second checkerboard surface comes from the geodesic disks in $P_\pm$ with slope one).

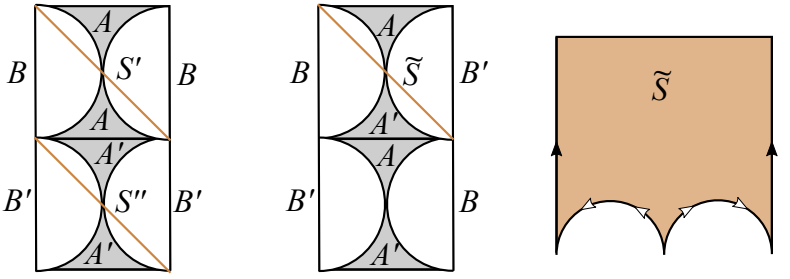

(*a*) Borromean rings (*b*) Twisted B-rings (*c*) Gluing on $\widetilde{S}$

Figure 11: Intersecting crossing disks in non-separating geodesics.

The fundamental domain in Figure 11(*b*) is for the Borromean rings with a half-twist in each crossing circle (compare gluing patterns with Figure 11(*a*)). The geodesic disk $\widetilde{S}$ is an ideal square whose edges are identified as in Figure 11(*c*), which yields a thrice-punctured sphere in the twisted Borromean rings.

The final example is rather lengthy, but supplies a complete classification of embedded, totally geodesic surfaces in an infinite family of link complements.

Example 5.2. The classification of embedded, totally geodesic surfaces in two-bridge, flat fully augmented links.

Let B_n be a two-bridge link with n twist regions, and an even number of crossings in each twist region. Fully augmenting B_n results in a flat FAL $\mathcal{A}_n$ which is one of two types, depending on whether n is even or odd. Figure 12 illustrates $\mathcal{A}_n$ for $n = 4, 5$, and can be easily generalized to arbitrary n. This section concludes by classifying embedded, totally geodesic surfaces in the complements of the flat FALs $\mathcal{A}_n$.

The techniques of Section 2 demonstrate that the circle packing in Figure 13(*a*) is associated to $\mathcal{A}_4$ (see [20, Section 6.4] for a thorough discussion). The reader can confirm that the circle packing for $\mathcal{A}_5$ is that of Figure 12(*a*) with five, rather than four, middle circles. The top of Figure 13(*b*) is P_+ for $\mathcal{A}_5$ after mapping vertex p to infinity via a Möbius transformation. Throughout this example the standard domain $\mathcal{F}$ will be obtained by letting P_- be the reflection of P_+ across its bottom vertical face (see bottom of Figure 13(*b*)).

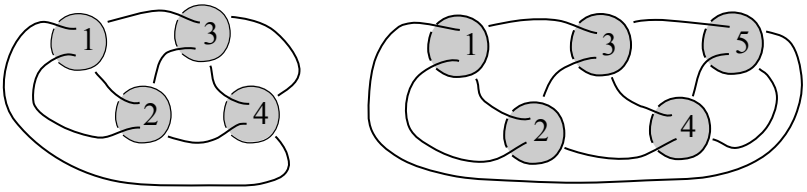

(*a*) The link $\mathcal{A}_4$ (*b*) The link $\mathcal{A}_5$

Figure 12: FALs coming from two-bridge links.

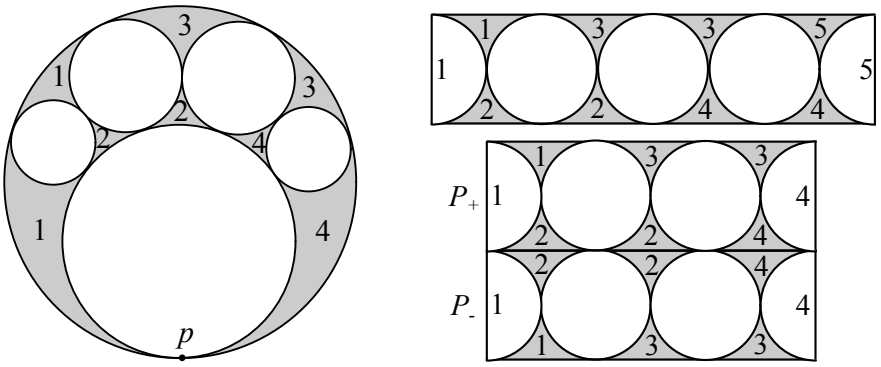

(*a*) Circle packing forB_4 (*b*) Odd P_+ and even $\mathcal{F}$

Figure 13: P_+ and $\mathcal{F}$ for two-bridge flat FALs.

Note that the left and right sides are *not* identified for this choice of P_+, which is perhaps atypical. The polyhedron P_+ for general $\mathcal{A}_n$ is in the form of Figure 13(b), with $n-2$ full circles in the middle. The left vertical shaded triangle in P_+ is always glued to the top adjacent triangle, as depicted. The right vertical shaded triangle glues to the bottom or top adjacent triangle depending on whether n is even or odd, respectively.

Before classifying surfaces, we limit the types of disks we must consider, taking advantage of the orthogonality restrictions given in Theorem 3.3 and Theorem 5.1.

By Theorem 3.3, geodesic disks that meet only unshaded faces must be contained in planes orthogonal to ∂P_+. It is not difficult to check that the

only hyperbolic planes orthogonal to ∂P_+ only along unshaded faces are depicted in Figure 14(a).

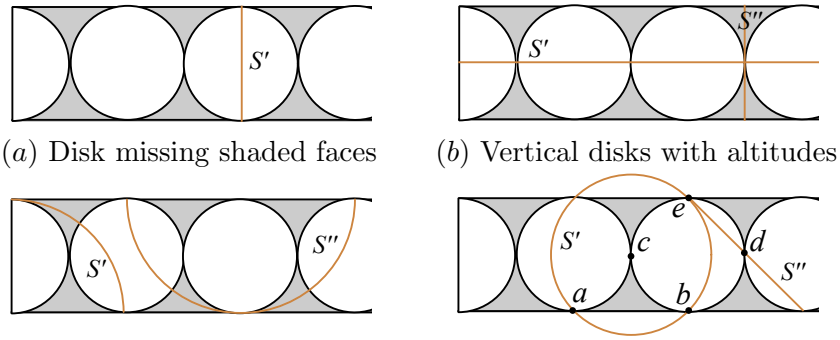

(a) Disk missing shaded faces (b) Vertical disks with altitudes

(c) Disks with altitudes (d) Disks with edges of ∂P_+

Figure 14: Potential geodesic disks in P_+.

There is a unique hyperbolic plane orthogonal to a shaded triangle along any altitude. In general these are not orthogonal to every face of ∂P_+; however, for our P_+ every altitude determines a hyperbolic plane intersecting ∂P_+ orthogonally. Vertical planes determined by altitudes yield the disks of Figure 14(b) and some representative disks coming from hemispherical planes are pictured in Figure 14(c). Note that the disk S' of Figure 14(c) also contains an altitude of the vertical shaded triangle on the left of P_+.

The final case to consider are geodesic disks that share an edge with ∂P_+. These are nowhere orthogonal to ∂P_+, which implies they do not contain an altitude and so must be an ideal n-gon.

Suppose S'' shares an edge with ∂P_+ and is contained in a vertical plane. The only such ideal n-gons, that are not orthogonal to ∂P_+, have boundary lines with slope ± 1 or they would have finite vertices. Hence S'' is of the form in Figure 14(d).

Now suppose S' is a geodesic disk in a hemispherical plane that contains the edge of ∂P_+ with endpoints a, b. As S' is an ideal n-gon, it must also contain the geodesic between b and one of the ideal vertices c, d or e of Figure 14(d). The disk containing a, b, c is standard, and a quick check shows that the disk containing a, b, d has finite vertices. Thus the only possibility for S' is the one pictured. A similar analysis shows a geodesic disk through

a point of tangency between middle circles (like c or d) must be contained in a vertical plane.

We now show that the disks of Figure 14(b) are not geodesic disks. To do so, note that the triangles labeled 1 in Figure 13(b) are identified. If the horizontal disk S' in Figure 14(b) projected to a totally geodesic surface, then S' would glue to another geodesic disk as in Figure 15(a) and the surface would not be embedded.

(a) No horizontal S' (b) No vertical S'

Figure 15: Ruling out potential geodesic disks.

Similarly, a disk like S'' of Figure 14(b) is not a geodesic disk. If it were, the gluing pattern would require that each vertical pair of shaded triangles have such a disk. Again, the triangles labeled 1 are identified forcing the addition of another disk as in Figure 15(b). The new disk intersects an existing one, making the projection non-embedded.

At this point we restrict our attention to the disks of Figure 14 parts (a), (c) and (d). It turns out that, with the right circumstances, each can project to embedded, totally geodesic surfaces.

Each disk of Figure 14(a) glues to its reflection to form a thrice punctured sphere in $\mathcal{A}_n$. These can be visualized in the link complement using Figure 12 as follows. Imagine each crossing disk as lying in a vertical plane. The region of the plane outside the disk is also a thrice punctured sphere.

The left- and right-most of these "outer" thrice-punctured spheres are isotopic to the crossing disks themselves, so there are a total of $n-2$ thrice-punctured spheres that miss crossing disks.

Both types of disks in Figure 14(c) can be geodesic disks. In either type of disk, one can readily verify that if all ideal vertices correspond to crossing circle punctures, then they and their reflections project to embedded, totally geodesic surfaces. Figure 16 illustrates this phenomenon for $\mathcal{A}_4$, where dots indicate ideal vertices that correspond to crossing circle punctures. The geodesic disks of Figure 16(a) project to thrice-punctured spheres,

while those of 16(b) to four-punctured spheres. This results in n more non-standard surfaces in $\mathcal{A}_n$, resulting in a total of $2n-2$ thus far.

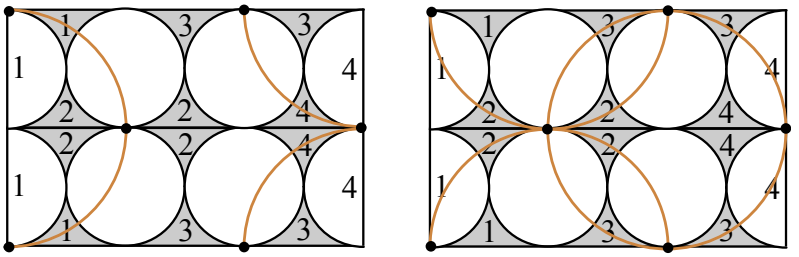

(a) 3-punctured spheres (b) 4-punctured spheres

Figure 16: Geodesic disks that project to embedded, totally geodesic surfaces in $\mathcal{A}_4$.

The disks of Figure 14(c) are not geodesic disks if they have ideal vertices corresponding to knot circles. In this situation, the gluing patterns generate self-intersection as in the case of Figure 14(b) disks.

It is interesting to see this directly from Figure 12, at least for two of the three types of knot circles in the links $\mathcal{A}_n$. A disk from Figure 14(c) would project to a surface S of the type described in Theorem 5.1(i). If a crossing disk D is punctured twice by the same knot circle then S would intersect D in two separating geodesics, and hence have self-intersection. Two of the three types of knot circles in $\mathcal{A}_n$ puncture a crossing disk twice, and can therefore not be punctures for the surfaces of Theorem 5.1(i).

Finally we consider which disks containing edges of ∂P_+ project to embedded, totally geodesic surfaces. Conveniently, all such disks meet ∂P_+ at an angle of $\pi/4$ (see Figure 14(d)). They project to a surface whose local picture along an edge f is shown in Figure 17(a), which indicates how geodesic disks must be positioned to glue together. The portion of S pictured will be covered by geodesic disks $S'_\pm$ in $P_\pm$ that glue along copies of f which are not reflections of each other. This observation allows use to create two more embedded, totally geodesic surfaces in the complement of $\mathcal{A}_n$.

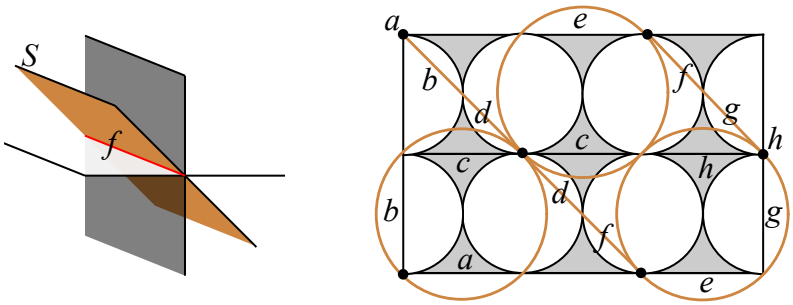

(a) Local picture of $S \cap \mathcal{C}$ (b) Geodesic disks for S

Figure 17: Geodesic disks that project to a non-standard surface in $\mathcal{A}_4$.

Figure 17(b) indicates how to construct the surfaces. Edges of $P_\pm$ with the same label are ones identified under gluing that give the local picture in Figure 17(a). Note that the labels a in the top left and h in the middle right refer to vertical edges on $P_\pm$. Also the label c in $P_\pm$ indicates a geodesic disk in that polyhedron meeting the edge c. The parabolic isometry gluing the shaded faces along c results in the desired local picture. It's a tedious exercise to confirm the remaining edges glue appropriately, resulting in an embedded, totally geodesic surface. This surface and its reflection across the plane of projection constitute the two non-standard surfaces in $\mathcal{A}_n$-complements that are not orthogonal to $\mathcal{C}$.

Thus there are a total of $2n$ non-standard surfaces in an $\mathcal{A}_n$ complement: $(n-2)$ satisfying Theorem 3.3, n which satisfy Theorem 5.1(i) and 2 that satisfy Theorem 5.1(ii). Of course, there are a total of n crossing disks, and either 2 or 3 reflection surface components, depending on if n is even or odd. In total, then, the complement of $\mathcal{A}_n$ has $3n+2$ embedded, totally geodesic surfaces if n is even, and $3n+3$ if n is odd.

6. Standard surfaces

There is considerable structure enjoyed by non-standard surfaces in FAL complements. Surfaces disjoint from crossing disks are very well understood, while those that intersect them are rather restricted in how they do so. It is natural to ask how complicated standard surfaces in FAL complements can be. Of course, crossing disks are standard and always thrice-punctured spheres, so the goal is to determine how complicated reflection surfaces can

be. If all crossing circles are flat, a picture will convince the reader that each connected component of the reflection surface is a punctured sphere. This observation, however, is deceptive. The purpose of this section is to construct very general reflection surfaces in FAL complements. More precisely, we will show that almost every checkerboard surface is totally geodesic in the appropriate augmentation of its boundary link.

The process of augmenting a checkerboard surface, which we now define, is key to understanding this result. Let R be a shaded checkerboard surface associated with a diagram D of a link L. If the bigons of a maximal twist region $\mathcal{T}$ of D are all part of R, we call $\mathcal{T}$ an *R-twist* (see Figure 18(a)). Alternatively, an *$\overline{R}$-twist* is a maximal twist region of D in which the bigons are not in R, as in Figure 18(b).

If $\mathcal{T}$ is an R-twist, augment it in the usual way by introducing a single crossing circle and removing full twists. If $\mathcal{T}$ is an $\overline{R}$-twist, place a crossing circle that is disjoint from R around each crossing in $\mathcal{T}$ (see Figure 18(b)).

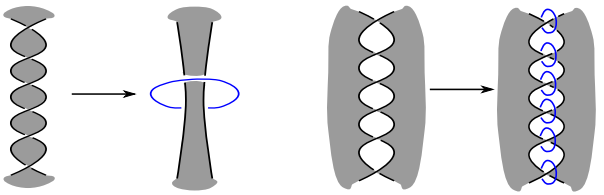

(a) $\mathcal{T}$ an R-twist (b) $\mathcal{T}$ an $\overline{R}$-twist

Figure 18: R-augmenting twist regions in D.

Definition 6.1. Let R be a checkerboard surface for a diagram D of the link L. The *R-augmentation of L* is the link $\mathcal{A}_R$ obtained by augmenting each maximal twist region as in Figure 18.

Note that the number of crossing circles in $\mathcal{A}_R$ is at least the number of twist regions in D, with equality if and only if every twist region in D is an R-twist. In this case the R-augmentation *is* the fully augmented link associated with D. This occurs, for example, when every twist region of D consists of a single crossing. Further note that the shaded surface in $\mathcal{A}_R$ is homeomorphic to R since the only difference is (possibly) removing full twists in bands. Both surfaces will be referred to as R, an abuse of notation that hopefully causes no confusion.

Of particular interest are those checkerboard surfaces whose augmentations are hyperbolic, and it turns out most of them will be. It may be helpful to review the diagrammatic properties described in Section 2, as well as the statement of Theorem 2.1.

Theorem 6.2. *Let R be a checkerboard surface for a nonsplittable, prime, twist-reduced diagram D with at least two twist regions. Then R is an embedded totally geodesic surface in the complement of the hyperbolic link $\mathcal{A}_R$.*

Proof. As R is a checkerboard surface for D, it is a reflection surface for $\mathcal{A}_R$. It is enough to show that $\mathcal{A}_R$ is hyperbolic, which will follow from demonstrating that it results from augmenting a diagram D' that satisfies the hypotheses of Theorem 2.1.

If all twist regions in D are R-twists then $\mathcal{A}_R$ is the result of fully augmenting D, which is assumed to satisfy the hypotheses of Theorem 2.1, and we are done. We turn our attention to checkerboard surfaces with at least one $\overline{R}$-twist.

If D contains $\overline{R}$-twists, then $\mathcal{A}_R$ is not the result of fully augmenting the diagram D. Nonetheless, we will show that $\mathcal{A}_R$ is the result of fully augmenting a related diagram D' that satisfies the hypotheses of Theorem 2.1, thereby proving that it is hyperbolic.

Choose Dehn fillings for the crossing circles of $\mathcal{A}_R$ so that the resulting diagram D' is alternating, agrees with D on R-twists, and filling each crossing circle from an $\overline{R}$-twist yields 3-crossings (compare Figure 19 parts (a) and (c)). Thus each $\overline{R}$-twist $\mathcal{T}$ of D corresponds to parallel 3-crossing twist regions in D', one 3-crossing twist region for each crossing in $\mathcal{T}$.

Constructing L' in this manner ensures that $\mathcal{A}_R$ is the result of fully augmenting D'. To conclude that $\mathcal{A}_R$ is hyperbolic, then, it suffices to verify that D' is non-split, prime, twist-reduced and has at least two twist regions.

Now D' has as many twist regions as $\mathcal{A}_R$ has crossing circles, which is more than the number of twist regions in D since D contains at least one $\overline{R}$-twist. Hence the diagram D' has more than two twist regions.

The diagrams D and D' agree on R-twists of D. If $\mathcal{T}$ is an $\overline{R}$-twist in D, one obtains D' by replacing each crossing of $\mathcal{T}$ with a three-crossing twist region that cuts "orthogonally" across $\mathcal{T}$. Reversing this process, removing a full twist from the appropriate three-crossing twist regions in D', one obtains D. This observation will be useful in proving the remaining properties of D'.

A splitting disk for D' is one whose boundary is disjoint from D' and which divides the plane into two pieces, both of which contain non-trivial portions of D'. Note that a splitting disk for D' would, after removing the

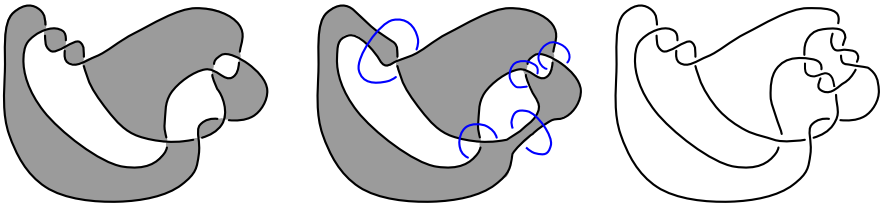

(a) Diagram D with R (b) The link $\mathcal{A}_R$ (c) The diagram D'

Figure 19: Augmenting a checkerboard surface and Dehn filling to get D'.

necessary full twists, also split D. Since D is nonsplittable the diagram D' must be as well.

To see that D' is prime we must show that every 2-tangle is trivial. If there were a 2-tangle in D' containing some (but not all) crossings in D', then the tangle would contain (at least) an entire twist region of D'. Retrieving D from D' always replaces three-crossing twist regions with one-crossing ones. Thus a non-trivial 2-tangle for D' would produce a non-trivial 2-tangle in D as well, a contradiction. Every 2-tangle in D' is trivial, as desired.

Finally we must show that D' is twist-reduced. Suppose the diagram D' admits a decomposition into two 4-tangles S and T with two exterior crossings as in Figure 1(b). We will show that one of the 4-tangles contains a twist. Note that the same S and T can be chosen to give such a decomposition of diagram D as well. Even if the exterior crossings are part of a three-crossing twist region in D' that reduces to a single crossing in D, simply choose the exterior crossing to be the one that remains.

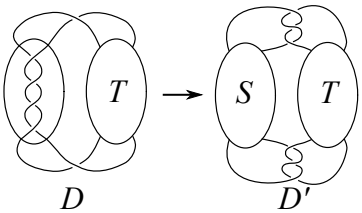

Figure 20: Constructing D' if S an $\overline{R}$-twist of D.

Since D is twist reduced one of the tangles, say S, must be a twist. In this case the exterior crossings are part of the same maximal twist region

$\mathcal{T}$. If $\mathcal{T}$ were an $\overline{R}$-twist, then creating D' results in twist regions outside S and T that cannot be absorbed into either tangle (see Figure 20). This contradicts the fact that S and T decompose D' into the form of Figure 1(b). Hence $\mathcal{T}$ must be an R-twist in D which implies that D and D' agree outside tangle T. The tangle S is then a twist in D', as desired.

The diagram D', then, satisfies the hypotheses of Theorem 2.1, and $\mathcal{A}_R$ is hyperbolic, completing the proof. □

References

[1] C.C. Adams, *Thrice-punctured spheres in hyperbolic 3-manifolds.* Trans. Amer. Math. Soc., **287** (1985), no. 2, 645–656.

[2] C.C. Adams, *Augmented alternating link complements are hyperbolic.* Low-dimensional topology and Kleinian groups (Coventry/Durham, 1984), London Math. Soc. Lecture Not Ser., Vol. **112**, Cambridge Univ. Press, Cambridge, (1986), 115–130.

[3] C.C. Adams, H. Bennett, C. Davis, M. Jennings, J. Kloke, N. Perry, E. Schoenfeld, *Totally geodesic Seifert surfaces in hyperbolic knot and link complements II.* J. Differential Geom., **79** (2008), no. 1, 1–23.

[4] C.C. Adams, J. Brock, J. Bugbee, T. Comar, K. Faigin, A. Huston, A. Joseph, D. Pesikoff, *Almost alternating links.* Topology Appl., **46** (1992), no. 2, 151–165.

[5] C.C. Adams, E. Schoenfeld, *Totally geodesic Seifert surfaces in hyperbolic knot and link complements I.* Geom. Dedicata, **116** (2005), 237–247.

[6] E. M. Andreev. *On convex polyhedra in Lobacevskii spaces (English Translation).* Math. USSR Sbornik, **10** (1970), 413–440.

[7] R. Blair, D. Futer, and M. Tomova, *Essential surfaces in highly twisted link complements.* Alg. Geom. Topol., **15** (2015), no. 3, 1501–1523.

[8] J. Calvo, *Knot enumeration through flypes and twisted splices.* J. Knot Theory and Ramificaitons, **6** (1997), no. 6, 785–798.

[9] E. Chesebro, J. DeBlois, H. Wilton, *Some virtually special hyperbolic 3-manifold groups.* Comment. Math. Helv., **87** (2012), no. 3, 727–787.

[10] D. Futer, E. Kalfagianni, J. Purcell, *Quasifuchsian state surfaces.* Trans. Amer. Math. Soc., **366** (2014), no. 8, 4323–4343.

[11] D. Futer, J. Purcell, *Links with no exceptional surgeries*. Comment. Math. Helv., **82** (3) (2007), 629–664.

[12] K. Ichihara, M. Ozawa, *Hyperbolic knot complements without closed embedded totally geodesic surfaces*. J. Austral. Math. Soc. Ser. A, **68** (2000), 379–386.

[13] E. Kalfagianni, C.R.S. Lee, *Crosscap numbers and the Jones Polynomial*. Adv. Math., **286** (2016), 308–337.

[14] M. Lackenby, *The volume of hyperbolic alternating link complements*. Proc. London Math. Soc. (3), **88** (2004), no. 1, 204–224, with an appendix by Ian Agol and Dylan Thurston.

[15] C. Maclachlan, A. Reid, *The arithmetic of hyperbolic 3-manifolds*. Springer-Verlag, New York, (2003).

[16] H. Matsuda, *Complements of hyperbolic knots of braid index four contain no closed embedded totally geodesic surfaces*. Topology Appl., **119** (2002), no. 1, 1–15.

[17] W. Menasco, A. Reid, *Totally geodesic surfaces in hyperbolic link complements*. Topology '90 (Columbus, OH, 1990), 215–226, Ohio State Univ. Math. Res. Inst. Pub., 1, de Gruyter, Berlin, 1992.

[18] P. Morgan, B. Ransom, D. Spyropoulos, R. Trapp, C. Ziegler, *Belted-sum decompositions of fully augmented links*. in preparation.

[19] J. Purcell, *An introduction to fully augmented links*. Contemporary Mathematics, Vol. **541** (2011), 205–220.

[20] J. Purcell, *Cusp shapes under cone deformations*. J. Differential Geometry, **80** (2008), 453–500.

[21] A. Reid, *Totally geodesic surfaces in hyperbolic three-manifolds*. Proc. Edin. Math. Soc. **34** (1991), 77–88.

Department of Mathematics, Georgia Institute of Technology
Atlanta, GA 30332, USA
E-mail address: sknavel3@gatech.edu

Department of Mathematics
California State University, San Bernardino
San Bernardino, CA 92407, USA
E-mail address: rtrapp@csusb.edu

Received May 22, 2020
Accepted December 8, 2020